IOPscience iopscience.iop.org

Home Search Collections Journals About Contact us My IOPscience

Local distortions in the colossal magnetoresistive manganates $La_{0.70}Ca_{0.30}MnO_3$, $La_{0.80}Ca_{0.20}MnO_3$ and $La_{0.70}Sr_{0.30}MnO_3$ revealed by total neutron diffraction

This article has been downloaded from IOPscience. Please scroll down to see the full text article.

1999 J. Phys.: Condens. Matter 11 9221

(http://iopscience.iop.org/0953-8984/11/47/308)

View the table of contents for this issue, or go to the journal homepage for more

Download details:
IP Address: 171.66.16.220
The article was downloaded on 15/05/2010 at 17:58

Please note that terms and conditions apply.

J. Phys.: Condens. Matter **11** (1999) 9221–9238. Printed in the UK PII: S0953-8984(99)06780-6

Local distortions in the colossal magnetoresistive manganates $La_{0.70}Ca_{0.30}MnO_3$, $La_{0.80}Ca_{0.20}MnO_3$ and $La_{0.70}Sr_{0.30}MnO_3$ revealed by total neutron diffraction

S J Hibble†, S P Cooper†, A C Hannon‡, I D Fawcett§ and M Greenblatt§

† Department of Chemistry, University of Reading, Whiteknights, Reading RG6 6AD, UK
‡ ISIS Facility, Rutherford Appleton Laboratory, Chilton, Didcot, Oxon OX11 0QX, UK
§ Department of Chemistry, Rutgers University, Piscataway, NJ 08854-8087, USA

E-mail: s.j.hibble@rdg.ac.uk, s.p.cooper@rdg.ac.uk, a.c.hannon@rl.ac.uk, fawcett@rutchem.rutgers.edu and martha@rutchem.rutgers.edu

Received 9 August 1999

Abstract. The manganates $La_{0.80}Ca_{0.20}MnO_3$, $La_{0.70}Ca_{0.30}MnO_3$ and $La_{0.70}Sr_{0.30}MnO_3$ exhibit the colossal magnetoresistive (CMR) effect. Total neutron diffraction was employed to yield information on both the average and local atomic structure of these disordered crystalline materials as a function of temperature. The average structures were determined from Rietveld analysis of the Bragg scattering. Information on the local structures was obtained by Fourier transformation of the total diffraction pattern to yield the total correlation function, $T(r)$. Particular attention is paid to changes in the Mn–O bond distances, which are widely believed to be important in the CMR effect. Jahn–Teller distortions of the MnO_6 octahedra are absent at the lowest temperatures in the metallic phase. As the temperature is raised towards the paramagnetic–semiconducting to ferromagnetic–metallic transition at T_c, $T(r)$ exhibits clear increases in the variance of Mn–O bond distances, which greatly exceed those expected from the increase in disorder due to atomic thermal motion. This is confirmed by comparing the behaviour of the three materials, which have different values for T_c. The advantage of studying the local structure directly by determining $T(r)$ from total neutron scattering, rather than extrapolating from the average to local structure from Bragg scattering studies, is demonstrated. Comparisons are made with the results obtained for the ordered compound $LaMnO_3$, which does not exhibit the CMR effect. The three CMR manganates studied here do not show a separation of the Mn–O distances into two well resolved sets above T_c as reported by other workers.

1. Introduction

The manganates $La_{1-x}A_xMnO_3$, where A is a divalent ion, have attracted widespread interest because many of these materials exhibit colossal magnetoresistance (CMR) behaviour [1]. The large changes in resistance appear to be associated with structural changes and the detailed nature of these structural changes has been the subject of widespread interest and study.

All these manganates adopt distorted variants of the perovskite structure in which manganese is surrounded by six oxygen near neighbours. The MnO_6 groups are close to perfect octahedra in the end members with $x = 1$, for example in $CaMn^{IV}O_3$, but become more distorted when x becomes smaller. In $Ca^{IV}MnO_3$ the Mn–O distances are 2×1.895 Å, 2×1.900 Å and 2×1.903 Å [2], but in $LaMn^{III}O_3$ there are four short Mn–O bonds, 2×1.907 Å and 2×1.968 Å, and two long bonds at 2.178 Å [3]. This can be explained by the fact that manganese in oxidation state III has an outer electronic configuration of d^4

0953-8984/99/479221+18$30.00 © 1999 IOP Publishing Ltd

(high spin) and is expected to be Jahn–Teller active, but manganese IV with an outer electronic configuration of d^3 would not be.

The situation at intermediate compositions is complicated. Generally for larger values of x ($x \geqslant 5/8$) ordered structures are produced with distinct Mn^{III} and Mn^{IV} sites around which the Mn–O distances behave as explained above. However, for smaller values of x ($x \leqslant 0.5$), the compounds $La_{1-x}A_xMnO_3$, although crystalline, are structurally disordered. This complicates structural studies. In particular it makes it difficult to follow the behaviour of Mn–O bond lengths as a function of temperature. This behaviour is of great interest, because it has been suggested that, at low temperature in the metallic phase, electrons are delocalized in a conduction band and the manganese atoms become equivalent, leading to a much reduced or even completely removed Jahn–Teller distortion of the MnO_6 octahedra.

Changes in the average Mn–O bond lengths as a function of temperature in a number of disordered manganates have been studied using standard crystallographic methods to model the Bragg scattering. These studies show that discontinuous changes in the Mn–O bond lengths occur at the temperature T_c of the transition from the (high temperature) paramagnetic–semiconducting phase to the (low temperature) ferromagnetic metallic phase. For example, Radaelli *et al* [4] carried out a very careful powder neutron diffraction study using Rietveld analysis of the Bragg scattering, and concluded that a Jahn–Teller distortion was still present at low temperature in $La_{0.75}Ca_{0.25}MnO_3$.

Clearly there are difficulties, and dangers, in extrapolating from average structures to local behaviour in these disordered manganates. A number of workers have therefore attempted to gain information on local structure using extended x-ray fine structure spectroscopy (EXAFS) and neutron diffraction to yield correlation functions. Booth *et al* [5] reached the conclusion that local Jahn–Teller distortions disappeared at low temperature from an EXAFS study in which they compared the variance σ^2_{Mn-O} for the Mn–O bond length distributions in $La_{1-x}Ca_xMnO_3$ ($x = 0.21$, 0.25 and 0.30) with those obtained for $LaMnO_3$ and $CaMnO_3$. At low temperature the value of σ^2_{Mn-O} for the CMR manganates approached the value obtained for $CaMnO_3$, a material in which there is no Jahn–Teller distortion of the Mn–O bonds (see above). As the temperature was increased towards T_c, σ^2_{Mn-O} increased rapidly, and above T_c all the lanthanum calcium manganates had similar σ^2_{Mn-O} values. Their explanation for this behaviour is that there is a transition from localized (polaron) states at high temperature to a state with delocalized electrons in which the manganese atoms become identical well below T_c. Billinge *et al* [6] reached similar conclusions, for a series of $La_{1-x}Ca_xMnO_3$ compounds, from the behaviour of the width of the O–O correlation at 2.75 Å. However, it has been suggested by Louca *et al* [7] from a study of the pair correlation function in $La_{1-x}Sr_xMnO_3$, derived from neutron diffraction, that the Jahn–Teller distortion remains, although much reduced, even at low temperature. A similar conclusion was reached by Lanzara *et al* in their EXAFS study of $La_{0.75}Ca_{0.25}MnO_3$ [8]. A more extended discussion of 'lattice effects' in these materials can be found in a review by Millis [9].

Ideally one should examine the changes in both the average and local structures which occur in CMR manganates as a function of temperature. In order to achieve this we have collected total neutron diffraction data for the manganates $La_{0.70}Ca_{0.30}MnO_3$, $La_{0.80}Ca_{0.20}MnO_3$ and $La_{0.70}Sr_{0.30}MnO_3$, using the LAD diffractometer at the Rutherford Appleton Laboratory. We have simultaneously determined the average structures, by Rietveld analysis of the Bragg scattering and obtained the total correlation function, $T(r)$, by Fourier transformation of the interference function. In this way, we aim to correlate changes in both the average and local structures of these manganates with the changes in electronic transport properties, which occur on cooling through the insulator to metal transition. This study

therefore contrasts with previous work in which either the local or average structures (but not both) have been studied as a function of temperature.

2. Theory

2.1. Total neutron diffraction

The basic quantity measured in a total neutron diffraction experiment is the differential cross section [10]

$$\frac{\mathrm{d}\sigma}{\mathrm{d}\Omega} = I(Q) = I^s(Q) + i(Q) \tag{1}$$

where $I^s(Q)$ is known as the self-scattering and $i(Q)$ is known as the distinct scattering. Q is the magnitude of the scattering vector (momentum transfer) for elastic scattering, given by

$$Q = \frac{4\pi \sin\theta}{\lambda}. \tag{2}$$

The distinct scattering may be Fourier transformed to give the total correlation function

$$T(r) = T^0(r) + \frac{2}{\pi}\int_0^\infty Qi(Q)M(Q)\sin(rQ)\,\mathrm{d}Q \tag{3}$$

$$T^0(r) = 4\pi r g^0\left(\sum_i c_l \bar{b}_l\right)^2 \tag{4}$$

where $M(Q)$ is a modification function (used to reduce termination ripples due to the finite maximum momentum transfer Q_{max} of the experimental data), $g^0(= N/V)$ is the macroscopic number density of scattering units, c_l the atomic fraction and $\bar{b}_l$ the coherent neutron scattering length for element l. The modification function used in this work is that due to Lorch [11]:

$$\begin{aligned} M(Q) &= \frac{\sin(Q\Delta r)}{Q\Delta r} && \text{for } Q < Q_{max} \\ &= 0 && \text{for } Q < Q_{max} \end{aligned} \tag{5}$$

where $\Delta r = \pi/Q_{max}$.

The contribution to the experimental data due to Mn–O bonds was modelled by using the following procedure: firstly the reciprocal-space contribution was calculated by use of the Debye equation,

$$i_{calc}(Q) = \frac{1}{N}\sum_j \sum_{j\neq k} \bar{b}_j \bar{b}_k \frac{\sin QR_{jk}}{QR_{jk}} \exp\left(\frac{-\langle u_{jk}^2\rangle Q^2}{2}\right) \tag{6}$$

where $\bar{b}_j$ and $\bar{b}_k$ are the scattering lengths of atoms Mn and O, R_{jk} is the interatomic distance between a given pair of atoms and $\langle u_{jk}^2\rangle$ is the mean square thermal variation in interatomic distance. The sum was normalized in every case to an average atom, by dividing by $N = 5$, the number of atoms in the ($La_{1-x}A_xMnO_3$) formula unit. Secondly $i_{calc}(Q)$ was Fourier transformed according to equation (3) to yield the real-space contribution. The Fourier transform was performed using the same modification function and Q_{max} as for the experimental data. In this way, the model includes the same real-space resolution function as the experimental data.

2.2. Isotropic temperature factors

If it is assumed that atomic displacements are isotropic then the effect of atomic thermal motions on the Bragg scattering from a crystal may be described in terms of isotropic temperature factors, B_d, where B_d is the isotropic temperature factor for the dth atomic site in the unit cell [12]. The Debye–Waller factor for the contribution to the single differential cross-section due to the pair of sites d, d' is then given by

$$\exp\left(-\left(\frac{B_d + B_{d'}}{8\pi^2}\right) Q^2/2\right). \tag{7}$$

Equating this Debye–Waller factor with that for total neutron diffraction (as given in equation (6)) gives

$$8\pi^2\langle u_{jk}^2\rangle = B_j + B_k. \tag{8}$$

This equation is correct only within the approximation that atomic displacements are both isotropic and uncorrelated. If the unit cell contains more than one atom of a particular element, then a suitable average of the isotropic temperature factors must be used to calculate the mean square variation in interatomic distance.

3. Experiment

3.1. Synthesis and characterization of samples

Samples of $La_{1-x}Ca_xMnO_3$ ($x = 0, 0.2, 0.3$) were prepared from La_2O_3 (Alfa Aesar, 99.99%, fired at 800 °C prior to use), $CaCO_3$ (Aldrich, 99+%) and $Mn(NO_3)_2$ (Aldrich, 49.7 wt% solution in dilute nitric acid). Stoichiometric amounts of the starting materials were dissolved in approximately 50 cm^3 4M HNO_3 to which an excess of citric acid (Aldrich, 99.5%) and ethylene glycol (Aldrich, 99+%) with respect to metal-complex formation was added. After all the reactants had dissolved, the solution was heated on a hot plate, resulting in the formation of a gel. The gel was dried at 300 °C, then heated to 600 °C to remove the organic matter and to decompose the nitrates. The resultant ash was pressed into pellets and fired at 1100 °C for 12 h in a platinum crucible. $La_{0.8}Ca_{0.2}MnO_3$ and $La_{0.7}Ca_{0.3}MnO_3$ were reground and heated at 1200 °C for 48 h and then cooled to room temperature in the furnace. $LaMnO_3$ was heated at 1200 °C under argon for 24 h. Powder x-ray diffraction patterns of the products revealed that they were single-phase materials. The sample of $La_{0.7}Sr_{0.3}MnO_3$ was prepared in the same manner as the lanthanum calcium manganates, but using $SrCO_3$ (Cerac, 99.5%) in place of $CaCO_3$.

3.2. Magnetic susceptibility and resistivity measurements

Magnetic susceptibilities were determined using a Quantum Design SQUID magnetometer. The data were collected at 100 G from high to low temperature (field cooled) from 300 to 10 K for $La_{1-x}Ca_xMnO_3$ and from 400 to 10 K for $La_{0.70}Sr_{0.30}MnO_3$. Resistivity measurements for the $La_{1-x}Ca_xMnO_3$ samples were made over the same temperature range using a standard four-probe method. Gold wire contacts were attached to the sample (a polycrystalline, sintered block) with silver paint. The transition temperatures for ferromagnetic ordering and the maxima in resistivity (for the calcium doped samples) were found to be at 198 K for $La_{0.80}Ca_{0.20}MnO_3$, 270 K for $La_{0.70}Ca_{0.30}MnO_3$ and 374 K for $La_{0.70}Sr_{0.30}MnO_3$.

3.3. Neutron diffraction

Time of flight (tof) powder neutron diffraction data were collected on the LAD diffractometer at ISIS, Rutherford Appleton Laboratory, Chilton, Didcot, UK [13]. The diffractometer was equipped with pairs of detector banks at 5, 10, 20, 35, 58, 90 and 150°. Powdered polycrystalline samples, 9.41 g of $La_{0.70}Ca_{0.30}MnO_3$, 9.54 g of $La_{0.80}Ca_{0.20}MnO_3$, 8.71 g of $La_{0.70}Sr_{0.30}MnO_3$ and 8.30 g of $LaMnO_3$ were loaded into cylindrical vanadium sample holders of 8 mm internal diameter. The effective atomic density of each sample, as used in the data correction routines, was determined from the sample depth. The samples were cooled using a closed cycle refrigerator. Data were collected over the time of flight range 100–19 750 μs and analysed using the Q range 0.25–50 Å^{-1}. Background runs were collected on the empty can, empty instrument and a standard vanadium rod.

4. Results

4.1. Rietveld analysis

Data for Rietveld analysis were obtained by combining the signals from the two 150° detector banks and normalizing to the neutron flux, as measured by the vanadium data. Rietveld refinements were carried out using the program TF12LS [14], over the tof range 2000–14 000 μs (equivalent to a d-spacing range of 0.373–2.612 Å, or a Q-range of 2.406–16.845 Å^{-1}), with the peak shape modelled by a pseudo-Voigt function convoluted with a double exponential function. The coherent neutron scattering lengths used for La, Ca, Sr, Mn and O were 0.8240×10^{-14} m, 0.625×10^{-14} m, 0.702×10^{-14} m, -0.373×10^{-14} m and 0.5803×10^{-14} m, respectively [15]. The initial values used in our refinement of the nuclear structures of $La_{0.70}Sr_{0.30}MnO_3$ and $LaMnO_3$ were taken from the atomic parameters reported for these compounds by Radaelli *et al* [4] and Hauback *et al* [16] respectively. The initial values used in our refinement of the nuclear structures of $La_{0.70}Ca_{0.30}MnO_3$ and $La_{0.80}Ca_{0.20}MnO_3$ were taken from the atomic parameters of Radaelli *et al* for $La_{0.75}Sr_{0.25}MnO_3$ [4]. The structural parameters obtained from Rietveld analysis of the Bragg scattering from $LaMnO_3$ at 15 K and $La_{0.70}Ca_{0.30}MnO_3$ over the temperature range 15–310 K are shown in table 1. The structural parameters for $La_{0.80}Ca_{0.20}MnO_3$ and $La_{0.70}Sr_{0.30}MnO_3$ over the temperature range 15–310 K are shown in tables 2 and 3 respectively. The results of one refinement, I_{obs}, I_{calc} and the difference plot, $(I_{obs} - I_{calc})$/esd, for $La_{0.70}Ca_{0.30}MnO_3$ at 15 K are shown in figure 1. The data from the 150° detector banks were used for the profile refinement because these have the best resolution and hence yield the most accurate nuclear parameters. However, the minimum Q for the data measured at 150° is relatively high and in fact the magnetic form factor of manganese [17] is not significant over most of the Q-range of the data measured at 150°. Hence the contribution due to magnetic scattering can safely be ignored in the profile refinement. Figure 1 shows that the model including nuclear scattering gives a good fit to the Bragg scattering even at the lowest temperature studied, when the contribution due to magnetic Bragg scattering is at its greatest.

4.2. Total neutron diffraction analysis

Total neutron diffraction patterns were obtained by merging the data from all 14 detector banks normalized to absolute units, after correcting for detector dead-time, multiple scattering, attenuation and inelasticity using the ATLAS suite of programs [10] and extrapolating to $Q = 0$ Å^{-1}.

Table 1. Refined structural parameters from the Rietveld refinement for $LaMnO_3$ and $La_{0.7}Ca_{0.3}MnO_3$. Space group = *Pnma*, Mn on (0, 0, 0.5), La, Ca and O(1) on (x, 0.25, z) and O(2) on (x, y, z). $R_{wp} = [\sum_i w_i|Y_i(\text{obs}) - Y_i(\text{calc})|^2 / \sum_i w_i Y_i(\text{obs})^2]^{1/2}$ is the weighted profile R factor, w_i is the weight for point i, Y_i is the intensity of point i. V is the unit cell volume and B is the isotropic temperature factor.

	$LaMnO_3$	$La_{0.7}Ca_{0.3}MnO_3$									
	15 K	15 K	100 K	170 K	200 K	225 K	240 K	250 K	260 K	270 K	300 K
a (Å)	5.67921(4)	5.45718(3)	5.45917(4)	5.46168(3)	5.46155(4)	5.46207(3)	5.46279(3)	5.46380(3)	5.46510(4)	5.46558(3)	5.46597(4)
b (Å)	7.70305(5)	7.71337(5)	7.71684(6)	7.71426(4)	7.72032(6)	7.71938(5)	7.71830(4)	7.71936(4)	7.72395(6)	7.72035(4)	7.72603(6)
c (Å)	5.54104(3)	5.47313(4)	5.47539(5)	5.48049(3)	5.47819(5)	5.48037(4)	5.48287(4)	5.48383(4)	5.48128(6)	5.48494(4)	5.48237(5)
V (Å^3)	242.405(3)	230.382(3)	230.665(3)	230.908(2)	230.987(3)	231.073 (3)	231.177(2)	231.292(2)	231.377(4)	231.444(2)	231.522(3)
Mn B (Å^2)	0.1	0.08(2)	0.10(3)	0.09(6)	0.13(3)	0.08(4)	0.14(3)	0.15(5)	0.20(2)	0.24(6)	0.22(2)
La/Ca x	0.0426(6)	0.0204(3)	0.0198(4)	0.0178(7)	0.0194(4)	0.0187(4)	0.0185(6)	0.187(6)	0.0187(3)	0.0185(6)	0.0197(3)
z	0.9945(8)	0.9958(7)	0.9955(7)	0.993(1)	0.9959(7)	0.9952(8)	0.994(1)	0.9932(9)	0.9949(5)	0.993(1)	0.9950(5)
B (Å^2)	0.1	0.13(2)	0.18(2)	0.25(4)	0.26(2)	0.28(3)	0.25(5)	0.29(4)	0.35(2)	0.27(5)	0.38(1)
O(1) x	0.4884(8)	0.4917(6)	0.4912(6)	0.491(1)	0.4916(6)	0.4910(8)	0.4918(7)	0.491(1)	0.4911(5)	0.490(1)	0.4913(5)
z	0.0711(2)	0.0661(6)	0.0657(6)	0.0613(9)	0.0654(6)	0.0629(7)	0.061(1)	0.0610(9)	0.0637(5)	0.0608(9)	0.0637(5)
B (Å^2)	0.1	0.32(3)	0.35(4)	0.39(6)	0.47(4)	0.59(5)	0.59(7)	0.57(6)	0.59(3)	0.51(7)	0.62(3)
O(2) x	0.3018(6)	0.2739(4)	0.2737(4)	0.2753(7)	0.2740(4)	0.2742(5)	0.2746(7)	0.2757(6)	0.2752(3)	0.2759(6)	0.2751(3)
y	0.0380(4)	0.0323(4)	0.0322(3)	0.0339(4)	0.0321(3)	0.0334(3)	0.0337(4)	0.0339(4)	0.0333(2)	0.0344(4)	0.0330(2)
z	0.7268(6)	0.7257(4)	0.7259(4)	0.7254(7)	0.7257(4)	0.7249(5)	0.7241(7)	0.7240(6)	0.7244(3)	0.7239(6)	0.7245(3)
B (Å^2)	0.1	0.29(2)	0.35(2)	0.49(5)	0.43(3)	0.44(3)	0.52(5)	0.60(5)	0.57(2)	0.54(5)	0.63(2)
R_{WP}	8.95	6.53	6.44	8.67	5.19	6.33	8.58	7.89	3.95	4.97	3.83

Table 2. Refined structural parameters from the Rietveld refinement for $La_{0.8}Ca_{0.2}MnO_3$. Space group = *Pnma*, Mn on (0, 0, 0.5), La, Ca and O(1) on (x, 0.25, z) and O(2) on (x, y, z).

	15 K	120 K	150 K	175 K	220 K	250 K	300 K	310 K
a (Å)	5.47140(2)	5.47353(2)	5.47472(2)	5.47862(3)	5.47967(7)	5.48034(6)	5.48036(3)	5.4804(1)
b (Å)	7.73384(4)	7.73923(3)	7.74179(3)	7.74872(5)	7.7495(1)	7.7513(1)	7.74834(5)	7.7478(2)
c (Å)	5.49766(3)	5.50008(2)	5.50172(2)	5.50259(4)	5.50384(8)	5.50505(7)	5.50624(3)	5.5059(1)
V (Å^3)	232.633(2)	232.988(2)	233.185(2)	233.598(3)	233.719(5)	233.853(5)	233.815(2)	233.786(9)
Mn B (Å^2)	0.01(3)	0.02(5)	0.04(4)	0.15(2)	0.19(2)	0.15(2)	0.05(3)	0.07(2)
La/Ca x	0.0183(6)	0.0176(7)	0.0179(5)	0.0199(3)	0.0197(3)	0.0191(3)	0.0184(6)	0.0182(6)
z	0.9938(9)	0.995(1)	0.9946(7)	0.9949(5)	0.9950(5)	0.9954(6)	0.9944(9)	0.9947(9)
B (Å^2)	0.04(4)	0.15(6)	0.22(3)	0.27(2)	0.35(2)	0.37(2)	0.25(4)	0.21(4)
O(1) x	0.491(1)	0.492(1)	0.4915(8)	0.4918(5)	0.4914(5)	0.4910(6)	0.491(1)	0.491(1)
z	0.0630(9)	0.061(1)	0.0625(7)	0.0650(4)	0.0640(5)	0.0634(5)	0.0627(9)	0.0632(9)
B (Å^2)	0.27(6)	0.38(8)	0.53(5)	0.49(3)	0.64(3)	0.72(4)	0.52(6)	0.49(7)
O(2) x	0.2736(6)	0.2734(8)	0.2726(5)	0.2736(3)	0.2744(3)	0.2741(4)	0.2742(6)	0.2744(2)
y	0.0339(4)	0.0346(5)	0.0343(3)	0.0336(2)	0.0342(2)	0.0344(2)	0.0349(4)	0.0348(4)
z	0.7267(6)	0.7268(8)	0.7265(5)	0.7263(3)	0.7259(3)	0.7257(3)	0.7254(6)	0.7256(6)
B (Å^2)	0.31(5)	0.56(7)	0.48(3)	0.55(2)	0.61(2)	0.60(3)	0.50(5)	0.43(5)
R_{WP}	10.55	9.86	7.60	4.06	4.56	4.78	7.62	7.87

Table 3. Refined structural parameters from the Rietveld refinement for $La_{0.7}Sr_{0.3}MnO_3$, space group = $R\bar{3}c$, Mn on (0, 0, 0), La and Sr on (0, 0, 0.25) and O on (x, 0, 0.25).

	15 K	80 K	170 K	230 K	270 K	300 K
a (Å)	5.50211(3)	5.50300(4)	5.50421(5)	5.50597(3)	5.50733(5)	5.50850(3)
c (Å)	13.34104(4)	13.34241(5)	13.35104(3)	13.36044(4)	13.36699(4)	13.37171(5)
V (Å^3)	349.767(3)	349.916(4)	350.296(5)	350.767(3)	351.113(5)	351.386(3)
Mn B (Å^2)	0.04(3)	0.02(3)	0.04(3)	0.09(3)	0.07(3)	0.11(3)
La/Sr B (Å^2)	0.13(2)	0.08(1)	0.14(2)	0.19(2)	0.19(2)	0.23(2)
O x	0.4578(1)	0.4577(1)	0.4580(1)	0.4584(1)	0.4588(2)	0.4589(1)
B (Å^2)	0.32(3)	0.37(1)	0.44(1)	0.51(1)	0.50(8)	0.58(1)
R_{WP}	6.53	7.26	6.87	6.38	6.44	5.86

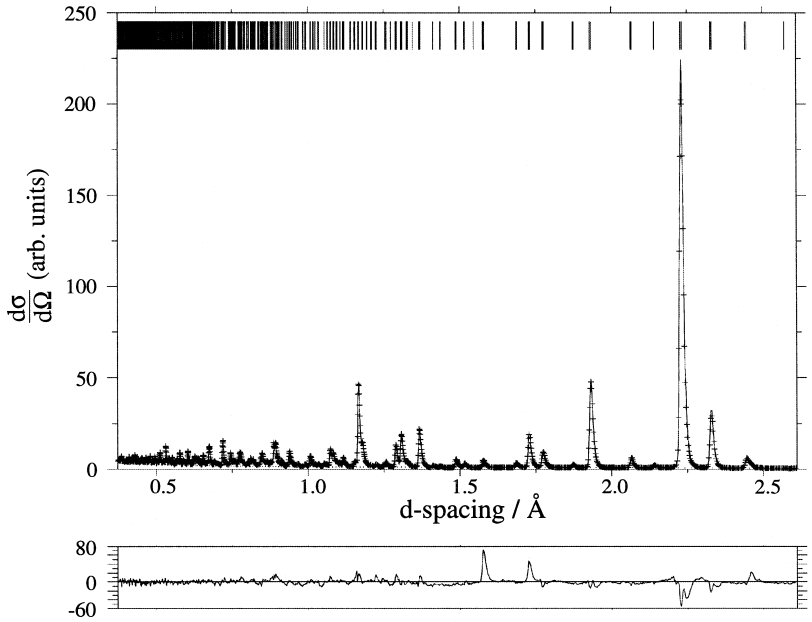

Figure 1. Final fitted profiles (points, observed; line, calculated; lower $(I_{obs} - I_{calc})$/esd) from Rietveld refinement for $La_{0.70}Ca_{0.30}MnO_3$ at 15 K. Tick lines directly above the diffraction pattern indicate the positions of the allowed reflections.

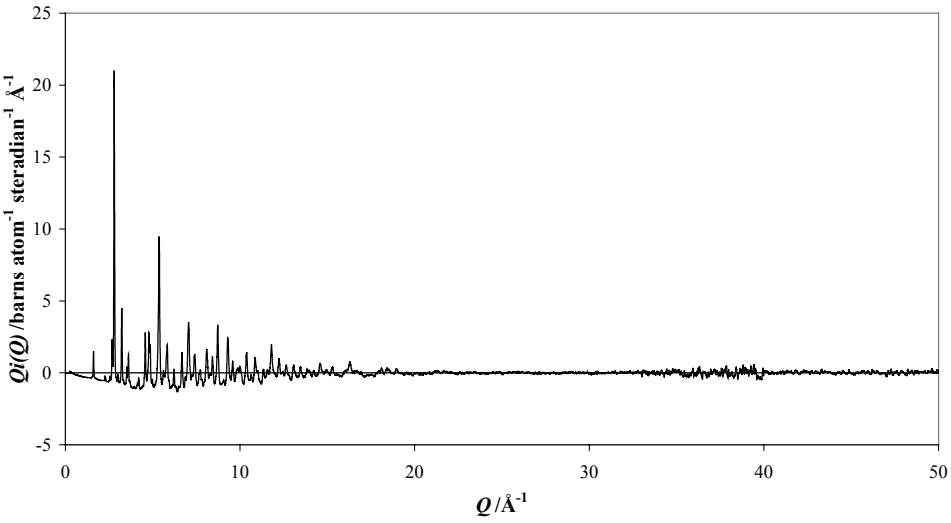

Figure 2. The interference function, $Qi(Q)$, for $La_{0.80}Ca_{0.20}MnO_3$ at 15 K.

The interference function, $Qi(Q)$, for $La_{0.80}Ca_{0.20}MnO_3$ at 15 K, out to $Q = 50$ Å^{-1}, is shown in figure 2. Note that at a scattering angle of 150° it was necessary to exclude a region 32.5–40 Å^{-1} in order to avoid a frame overlap contribution from a Bragg peak at $Q \approx 1.63$ Å^{-1} and this leads to the increased noise in this region of the interference function.

Table 4. Mn–O bond lengths for the disordered manganates, $La_{0.70}Ca_{0.30}MnO_3$, $La_{0.80}Ca_{0.20}MnO_3$ and $La_{0.70}Sr_{0.30}MnO_3$ and the model compounds $LaMnO_3$ and $CaMnO_3$.

Compound	Space group	Temperature (K)	Mn–O bond length (Å)
$LaMnO_3$	*Pnma*	15	$2 \times 1.909(3)$
			$2 \times 1.9668(3)$
			$2 \times 2.145(3)$
$CaMnO_3$ [2]	*Pnma*	300	$2 \times 1.895(1)$
			$2 \times 1.900(1)$
			$2 \times 1.903(1)$
$La_{0.70}Ca_{0.30}MnO_3$	*Pnma*	15	$2 \times 1.9625(6)$
			$2 \times 1.955(2)$
			$2 \times 1.959(2)$
		300	$2 \times 1.9634(5)$
			$2 \times 1.960(1)$
			$2 \times 1.964(1)$
$La_{0.80}Ca_{0.20}MnO_3$	*Pnma*	15	$2 \times 1.9649(9)$
			$2 \times 1.965(3)$
			$2 \times 1.965(3)$
		300	$2 \times 1.9682(9)$
			$2 \times 1.968(3)$
			$2 \times 1.973(3)$
$La_{0.70}Sr_{0.30}MnO_3$	$R\bar{3}c$	15	$6 \times 1.9526(4)$
		300	$6 \times 1.9549(4)$

5. Modelling and discussion

5.1. The average structure

5.1.1. $LaMnO_3$. The atomic co-ordinates and lattice parameters, table 1, obtained from Rietveld analysis for $LaMnO_3$ are in good agreement with those obtained by other workers [3]. However, we had to fix the isotropic thermal parameters B at 0.1 Å^2 to achieve a stable refinement. The derived Mn–O bond lengths, table 4, clearly show the Jahn–Teller distortion of the MnO_6 octahedra, with four short and two long Mn–O bonds. Table 4 also gives the literature values for the end-member model compound $CaMnO_3$ [2] for comparison purposes.

5.1.2. $La_{0.70}Ca_{0.30}MnO_3$, $La_{0.80}Ca_{0.20}MnO_3$ and $La_{0.70}Sr_{0.30}MnO_3$. The atomic and lattice parameters obtained from Rietveld analysis for $La_{0.70}Ca_{0.30}MnO_3$, table 1, $La_{0.80}Ca_{0.20}MnO_3$, table 2 and $La_{0.70}Sr_{0.30}MnO_3$, table 3 are in good agreement with those obtained by Radaelli *et al* for $La_{0.75}Ca_{0.25}MnO_3$ and $La_{0.7}Sr_{0.3}MnO_3$ although of slightly lower precision. Table 4 gives the Mn–O bond lengths at the lowest and highest temperature studied for each of these materials. It is clear that the average structure, determined by profile refinement of the Bragg diffraction data, shows no sign of the large Jahn–Teller distortion seen for $LaMnO_3$. Indeed in the case of $La_{0.70}Sr_{0.30}MnO_3$ crystallographic symmetry imposes the restriction that all Mn–O bonds are of equal length. Figure 3 shows the behaviour of unit cell volume for $La_{0.70}Ca_{0.30}MnO_3$, $La_{0.80}Ca_{0.20}MnO_3$ and $La_{0.70}Sr_{0.30}MnO_3$. A change in the rate of variation of the unit cell volume occurs at T_c. This is in agreement with the study by Radaelli *et al* of $La_{0.75}Ca_{0.25}MnO_3$. They also found a discontinuity in the contraction of the mean Mn–O bond length at T_c. Although we see this discontinuity too, the errors in our bond lengths determined by Rietveld refinement are larger than those of Radaelli *et al*, reducing the significance of our result.

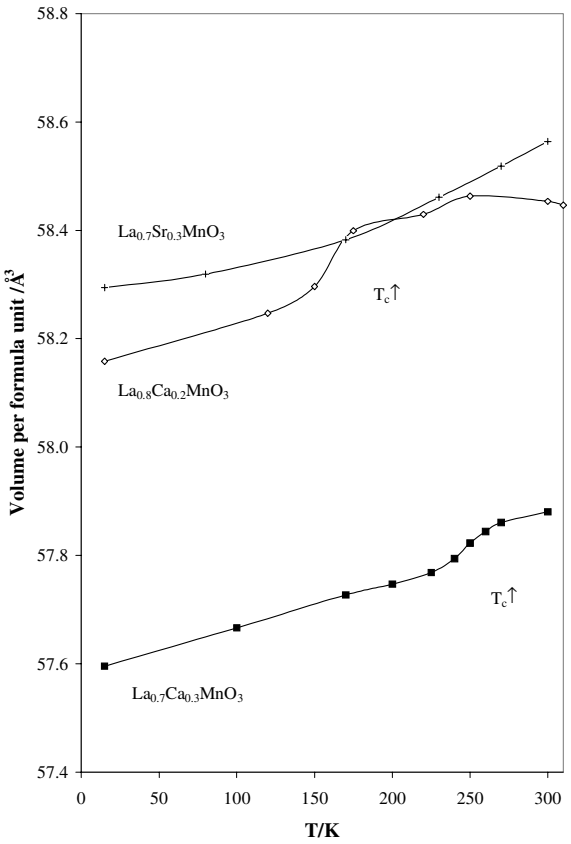

Figure 3. The behaviour of the volume per formula unit for $La_{0.70}Ca_{0.30}MnO_3$ (filled squares), $La_{0.80}Ca_{0.20}MnO_3$ (diamonds) and $La_{0.70}Sr_{0.30}MnO_3$ (crosses), as a function of temperature.

Radaelli *et al* plotted a Jahn–Teller distortion parameter

$$\sigma_{JT} = \sqrt{\frac{1}{3}\sum_i (R_{MnO,i} - \langle R_{MnO}\rangle)^2} \tag{9}$$

where $R_{MnO,i}$ is the ith Mn–O bond length and $\langle R_{MnO}\rangle$ is the mean Mn–O bond length. σ_{JT} gives a measure of the distortion of the MnO_6 octahedra. It is notable that they found this distortion parameter to be smaller above T_c than below. Radaelli *et al* therefore concluded that σ_{JT} on its own did not give a good measure of distortions in the MnO_6 octahedra because local distortions are incoherent with respect to the space group symmetry. Indeed the σ_{JT} values of Radaelli *et al* of 0.004 Å at low temperature and 0.003 Åat high temperature are close to that calculated, 0.0033 Å, for $CaMnO_3$ [2], which contains only Mn^{IV} and in which there is no Jahn–Teller distortion. Radaelli *et al* therefore went on to use the variation in the oxygen thermal parameters to give a measure of local distortions in the MnO_6 octahedra. Total neutron diffraction allows a direct determination of Mn–O bond distances and avoids falling back on this type of secondary evidence.

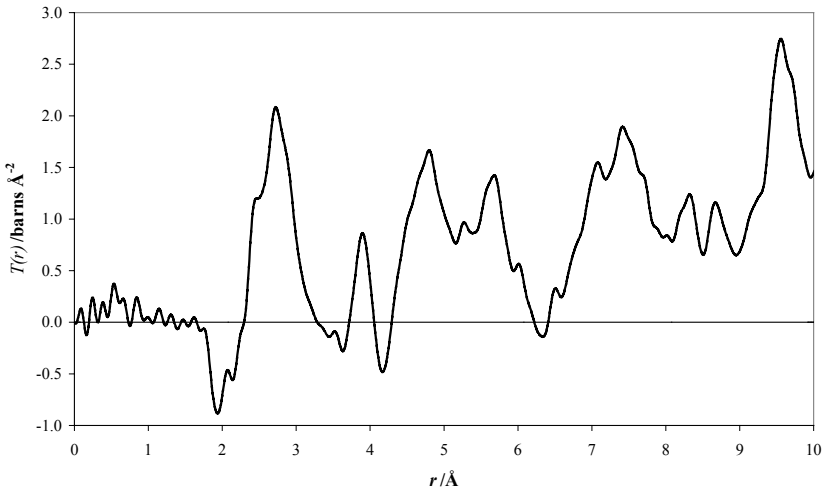

Figure 4. The experimentally determined total correlation function, $T(r)_{exp}$, from $r = 0$ to 10 Å, for $LaMnO_3$ at 15 K.

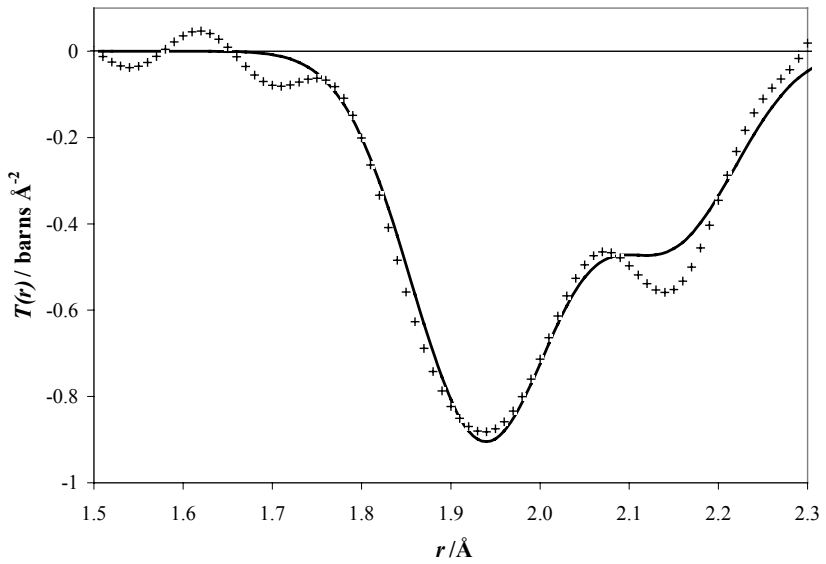

Figure 5. The experimentally determined total correlation function, $T(r)_{exp}$ (crosses), for $LaMnO_3$ from $r = 1.5$ to 2.3 Å, at 15 K and that produced, $T(r)_{calc}$ (line), from the structural parameters obtained by Rietveld refinement using $\langle u^2_{MnO} \rangle = 0.004$ Å^2.

5.2. The local structure

5.2.1. $LaMnO_3$. We first illustrate how total neutron diffraction gives the correct local information in the case of an ordered model compound. Figure 4 shows the experimentally determined total correlation function, $T(r)_{exp}$ for $LaMnO_3$ at 15 K. The agreement between $T(r)_{calc}$ and $T(r)_{exp}$ in the region where only Mn–O correlations occur (1.7–2.3 Å), see figure 5, is good for this ordered material. The model $T(r)_{calc}$ was calculated from the

structural parameters obtained by Rietveld refinement given in table 1, and using a single value of 0.004 Å^2 for the mean square thermal variation in Mn–O distance, $\langle u^2_{MnO}\rangle$. Note that Mn–O correlations give rise to a negative peak in $T(r)$, because manganese has a negative neutron scattering length. The two long Mn–O distances are clearly differentiated from the four shorter Mn–O distances in the Jahn–Teller distorted $Mn^{III}O_6$ octahedra. Note that we have not attempted to model the higher r region where other correlations become non-zero. This would be much more complicated because each partial correlation function requires a different value for $\langle u^2\rangle$. We have chosen in this work to concentrate on the Mn–O correlations, since these give a direct measure of local Jahn–Teller distortions.

5.2.2. $La_{0.70}Ca_{0.30}MnO_3$, $La_{0.80}Ca_{0.20}MnO_3$ and $La_{0.70}Sr_{0.30}MnO_3$. Figure 6 shows the experimentally determined total correlation function, $T(r)_{exp}$, over the r range 1.5–2.3 Å, as a function of temperature for $La_{0.70}Ca_{0.30}MnO_3$, $La_{0.80}Ca_{0.20}MnO_3$ and $La_{0.70}Sr_{0.30}MnO_3$. In all cases we found only one peak due to Mn–O correlations around 2 Å. This differs from the situation we found in the ordered compound $LaMnO_3$ where there are two classes of short and long Mn–O bonds in the MnO_6 octahedra, which are clearly resolved. Our results for $La_{0.70}Sr_{0.30}MnO_3$ disagree with the results of Louca *et al* [7], who found two distinct sets of Mn–O bonds in their study of $La_{1-x}Sr_xMnO_3$ ($0 \leqslant x \leqslant 0.4$) with a component at high r ($r > 2.15$ Å) similar to that found for $LaMnO_3$. It is also clear from figure 6 that the variance in the Mn–O bond lengths, as a function of temperature, behaves differently for the three compounds. At low temperature the width of the peak due to Mn–O correlations is almost the same for $La_{0.70}Ca_{0.30}MnO_3$, $La_{0.80}Ca_{0.20}MnO_3$ and $La_{0.70}Sr_{0.30}MnO_3$, see figure 6(a). The general trend is that the peaks in $T(r)$ become broader as the temperature increases for all of the compounds studied. A broadening of the peaks in $T(r)$ as the temperature is increased is to be expected, due to the increase in thermal motion of the atoms, and is not noteworthy in itself. However, the important feature to note is that the peak due to Mn–O correlations does not broaden with temperature at the same rate for each compound. For example, this peak broadens more for $La_{0.80}Ca_{0.20}MnO_3$ at a lower temperature than is the case for $La_{0.70}Ca_{0.30}MnO_3$ and $La_{0.70}Sr_{0.30}MnO_3$. This can be seen in figure 6(b) for $T(r)$ at 170 K. It appears that for each compound a large increase in the width of the peak due to Mn–O correlations occurs as T_c is approached from below. This suggests that a large amount of additional disorder is introduced into the Mn–O bond lengths at this stage and is consistent with the introduction of local Jahn–Teller distortions. For $La_{0.80}Ca_{0.20}MnO_3$ a more gradual increase in peak widths occurs above T_c. Above T_c $La_{0.80}Ca_{0.20}MnO_3$ and $La_{0.70}Ca_{0.30}MnO_3$ again have similar Mn–O peak widths. Thus at 300 K, which is above T_c for $La_{0.80}Ca_{0.20}MnO_3$ and $La_{0.70}Ca_{0.30}MnO_3$, the Mn–O peak widths for these two compounds are similar but much greater than for $La_{0.70}Sr_{0.30}MnO_3$.

To test whether there is a significant Jahn–Teller distortion in $La_{0.70}Sr_{0.30}MnO_3$ at 15 K, we calculated $T(r)$ from the Rietveld parameters in table 3 using the same $\langle u^2_{MnO}\rangle$ value of 0.004 Å^2 as used for the ordered compound, $LaMnO_3$. Figure 7(a) shows a comparison of the model correlation function, $T(r)_{calc}$, with the experimental data, $T(r)_{exp}$, for $La_{0.70}Sr_{0.30}MnO_3$. The good agreement shows that at 15 K the Mn–O bond lengths are correctly determined in the Rietveld refinement and there appear to be no significant local distortions. The value of 0.004 Å^2 used for $\langle u^2_{MnO}\rangle$ corresponds to an isotropic temperature factor, B (see equation (8)), of 0.32 Å^2, in good agreement with the values determined by Rietveld refinement (see table 3). Figure 7(b) shows a similar comparison for $La_{0.70}Sr_{0.30}MnO_3$ at a temperature of 300 K, using a value of 0.0074 Å^2 for $\langle u^2_{MnO}\rangle$ which was calculated from the oxygen B factor determined from the Rietveld refinement.

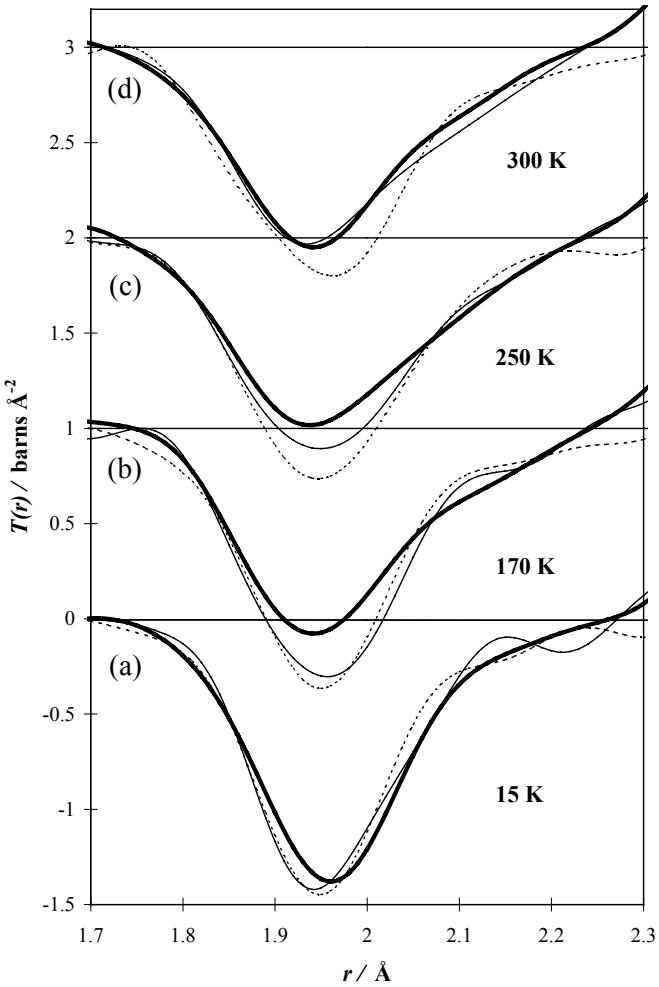

Figure 6. The experimentally determined total correlation function, $T(r)_{exp}$, at selected temperatures for $La_{0.70}Ca_{0.30}MnO_3$ (T_c = 270 K) (thin line), $La_{0.80}Ca_{0.20}MnO_3$ (T_c = 198 K) (thick line) and $La_{0.70}Sr_{0.30}MnO_3$ (T_c = 374 K) (dashed line). Temperature increases up the page and samples are at the temperature shown, except for $La_{0.80}Ca_{0.30}MnO_3$ at 175 K in (b) and $La_{0.70}Sr_{0.30}MnO_3$ at 270 K in (c). Plots (b), (c) and (d) are offset vertically by 1, 2 and 3 respectively.

A similar treatment was performed for $La_{0.80}Ca_{0.20}MnO_3$ and the results at 120 K (well below T_c) and 300 K (above T_c) are shown in figure 9. Good agreement between $T(r)_{exp}$ and $T(r)_{calc}$ was obtained at 120 K using a value $\langle u^2_{MnO}\rangle = 0.005$ Å^2 (obtained by interpolating the Rietveld B values for $La_{0.70}Sr_{0.30}MnO_3$) for Mn–O bonded correlations. It can again be seen that at 300 K the Mn–O correlations show evidence for Jahn–Teller distortions, with a long tail in $T(r)_{exp}$ developing to high r.

Figure 8(a) shows a similar treatment for $La_{0.70}Ca_{0.30}MnO_3$ at 15 K, using a value of 0.004 Å^2 for $\langle u^2_{MnO}\rangle$. Here again the model correlation function, $T(r)_{calc}$, calculated from the average structure determined in the Rietveld refinement, agrees reasonably well with the experimental result, $T(r)_{exp}$. In this case there are three different Mn–O bond lengths (see

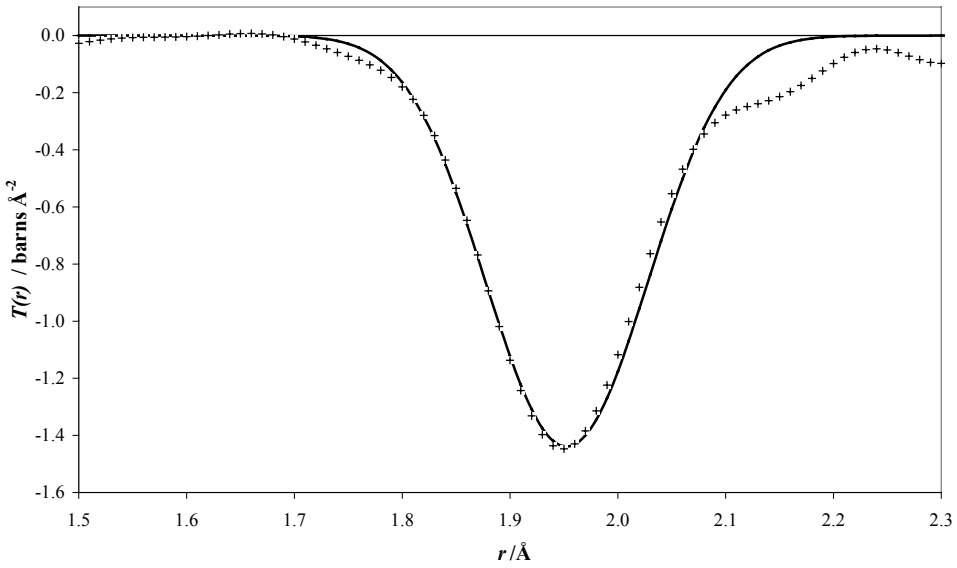

(a)

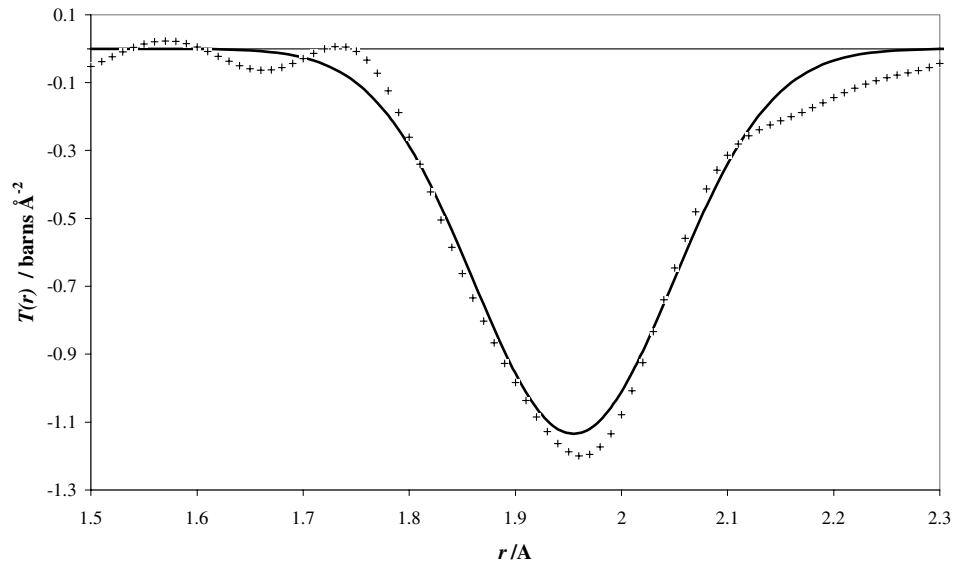

(b)

Figure 7. The total correlation function for $La_{0.70}Sr_{0.30}MnO_3$ at (a) 15 K and (b) 300 K. The experimental correlation function, $T(r)_{exp}$, is shown by crosses, whilst the model correlation function, $T(r)_{calc}$, is shown by a line. The model calculation used the structural parameters obtained by Rietveld refinement, given in table 3, with values for $\langle u^2_{MnO}\rangle$ of 0.004 Å^2 at 15 K and 0.0074 Å^2 at 300 K respectively.

table 4) in our model, but they are very close together and do not represent a Jahn–Teller distortion.

Figure 8(b) shows $T(r)_{exp}$ for $La_{0.70}Ca_{0.30}MnO_3$ at 300 K and the model function, $T(r)_{calc}$, which was calculated using the same value $\langle u^2_{MnO}\rangle = 0.0074$ Å^2, which was previously used

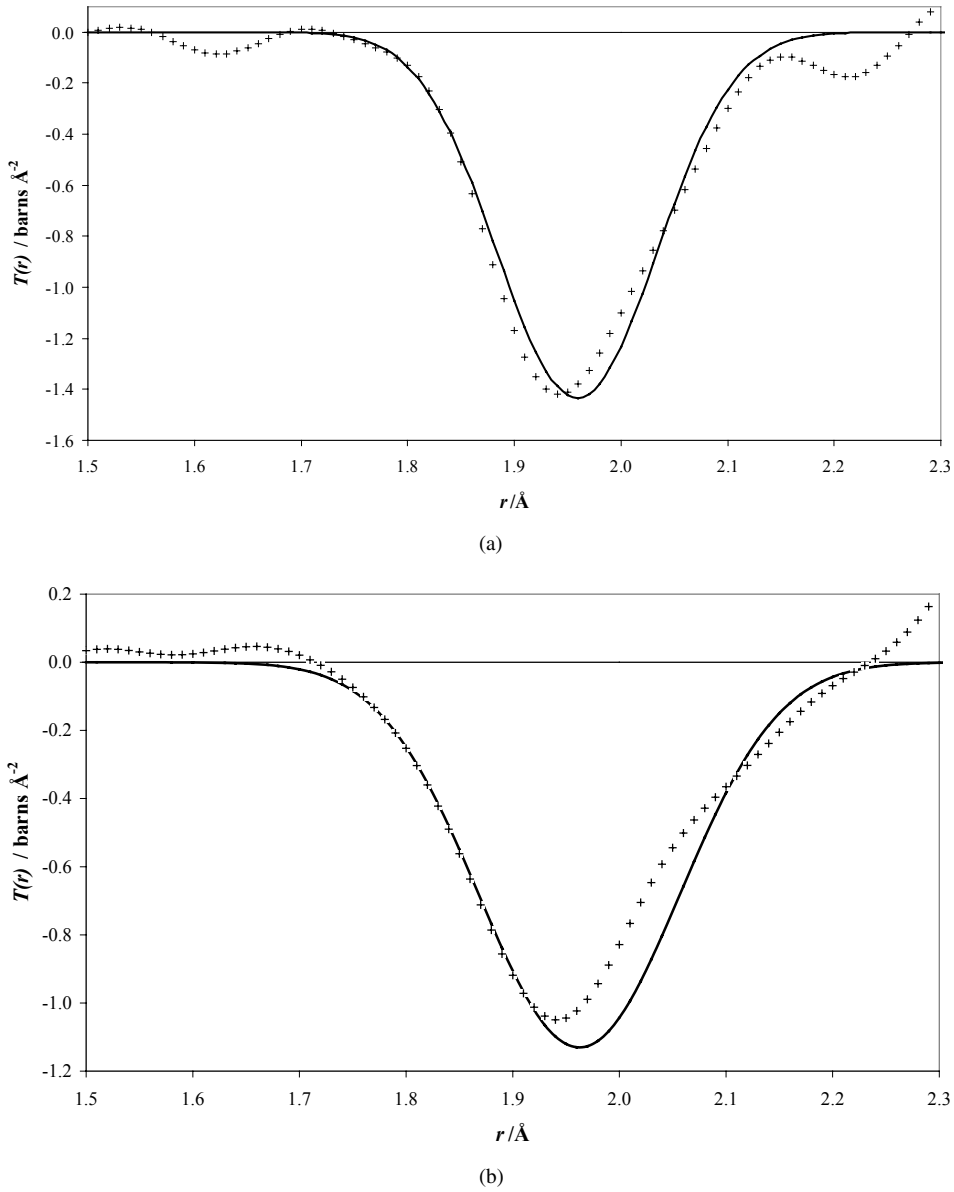

Figure 8. The total correlation function for $La_{0.70}Ca_{0.30}MnO_3$ at (a) 15 K and (b) 300 K. The experimental correlation function, $T(r)_{exp}$, is shown by crosses, whilst the model correlation function, $T(r)_{calc}$, is shown by a line. The model calculation used the structural parameters obtained by Rietveld refinement, given in table 1, with values for $\langle u^2_{MnO}\rangle$ of 0.004 Å^2 at 15 K and 0.0074 Å^2 at 300 K respectively.

to model $T(r)$ for $La_{0.70}Sr_{0.30}MnO_3$ at this temperature. This model gives poor agreement with the experimentally determined $T(r)_{exp}$. In fact it is impossible to model this peak well using any value of $\langle u^2_{MnO}\rangle$ with the bond lengths determined using Rietveld refinement. The advantage of comparing the experimentally determined $T(r)_{exp}$ with this model is that it shows clearly how the average structure from Rietveld refinement provides incorrect Mn–O bond lengths. It also shows that the increased variance in Mn–O bond lengths, above that

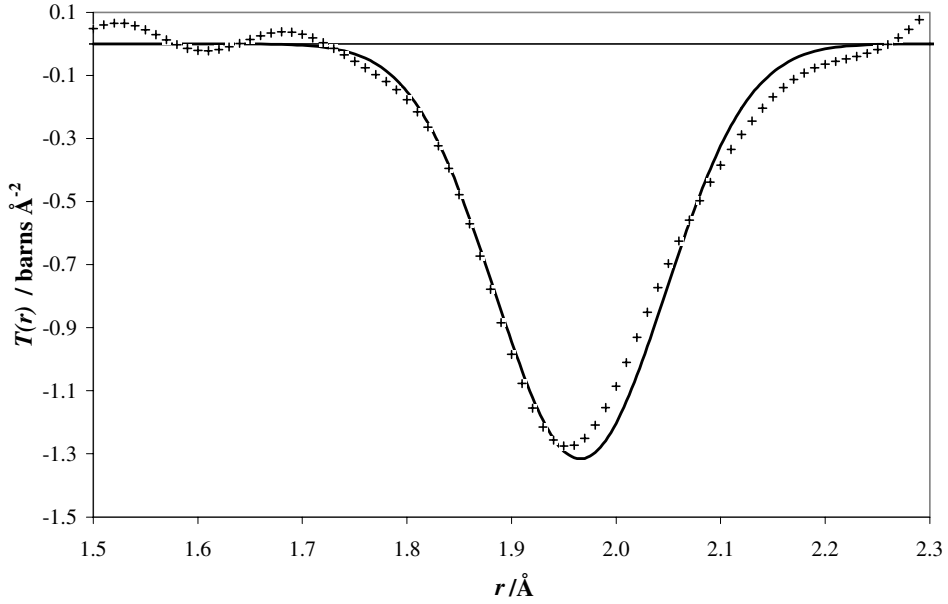

(a)

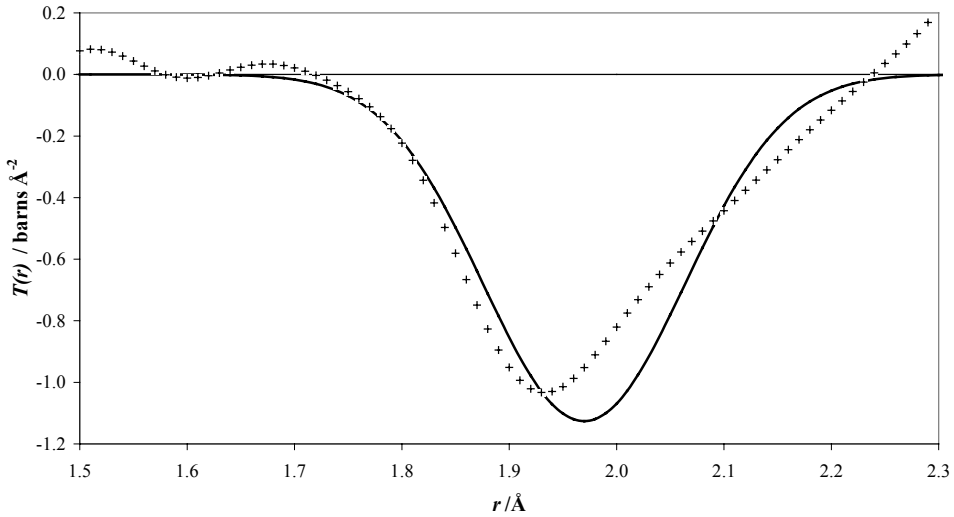

(b)

Figure 9. The total correlation function for $La_{0.80}Ca_{0.20}MnO_3$ at (a) 120 K and (b) 300 K. The experimental correlation function, $T(r)_{exp}$, is shown by crosses, whilst the model correlation function, $T(r)_{calc}$, is shown by a line. The model calculation used the structural parameters obtained by Rietveld refinement, given in table 2, with values for $\langle u^2_{MnO}\rangle$ of 0.005 Å^2 at 120 K and 0.0074 Å^2 at 300 K respectively.

expected from thermal broadening, is due to a tail which has developed on the high r side of the Mn–O peak in the experimental correlation function, $T(r)_{exp}$, for $La_{0.70}Ca_{0.30}MnO_3$ at 300 K. This tail shows that the Mn–O bonds are beginning to split into different populations, perhaps the long and the short bonds expected if local Jahn–Teller distortions occur.

Although in both $La_{0.70}Ca_{0.30}MnO_3$ and $La_{0.80}Ca_{0.20}MnO_3$ we see evidence for the onset of local Jahn–Teller distortions in the MnO_6 octahedra as we approach T_c from below, we must emphasize that we do not see, even above T_c, two clear populations of short and long bonds.

6. Conclusions

Determinations of both the average and local structures show that the distribution of Mn–O bond lengths in the disordered CMR manganates, $La_{0.80}Ca_{0.20}MnO_3$, $La_{0.70}Ca_{0.30}MnO_3$ and $La_{0.70}Sr_{0.30}MnO_3$ is much narrower than in $LaMnO_3$. Jahn–Teller distortions of the MnO_6 octahedra appear to be absent at 15 K, the lowest temperature we studied in the disordered manganates, and at this temperature the average structure determined from Rietveld modelling of the Bragg scattering correctly determines the distribution of Mn–O bond lengths. As the temperature approaches T_c, the variance in Mn–O bond lengths seen in $T(r)_{exp}$ increases much more rapidly than expected from purely thermal broadening. This increase is consistent with the occurrence of local Jahn–Teller distortions of the MnO_6 octahedra. However, even above T_c we do not see the separation of Mn–O bond lengths into two clear sets of short ($R_{MnO} \sim 1.95$ Å) and long ($R_{MnO} \sim 2.15$ Å) distances. The materials appear to be more structurally complex than simple models suggest. It is likely that in the disordered manganates at high temperature the frustration due to the random non-periodic distribution of the (Jahn–Teller active) Mn^{3+} sites and (Jahn–Teller inactive) Mn^{4+} sites prevents the transition to a structure with two distinct sets of Mn–O bond lengths.

References

[1] Rao C N R and Aruraj A 1998 *Curr. Opin. Solid State Mater. Sci.* **3** 23–31
[2] Poeppelmeier K R, Leonowicz M E, Scanlon J C and Longo J M 1982 *J. Solid State Chem.* **45** 71–9
[3] Rodriguez-Carvajal J, Hennion M, Moussa F and Moudden A 1998 *Phys. Rev.* B **57** 3189–92
[4] Radaelli P G, Iannone G, Marezio M, Hwang H Y, Cheong S W, Jorgensen J D and Argyriou D N 1997 *Phys. Rev.* B **56** 8265–76
[5] Booth C H, Bridges F, Kwei G H, Lawrence J M, Cornelius A L and Neumeier J J 1998 *Phys. Rev. Lett.* **80** 853–6
[6] Billinge S J L, DiFransesco R G, Kwei G H, Neumeier J J and Thompson J D 1996 *Phys. Rev. Lett.* **77** 715–18
[7] Louca D, Egami T, Brosha E L, Röder H and Bishop A R 1997 *Phys. Rev.* B **56** 8475–8
[8] Lanzara A, Saini N L, Brunelli M, Natali F, Bianconi A, Radaelli P G and Cheong S W 1998 *Phys. Rev. Lett.* **81** 878–81
[9] Millis A J 1998 *Nature* **392** 147–50
[10] Hannon A C, Howells W S and Soper A K 1990 *(IOP Conf. Ser. 107)* (Bristol: Institute of Physics) pp 193–211
[11] Lorch E 1969 *J. Phys. C: Solid State Phys.* **2** 229–37
[12] Willis B T M and Pryor A W 1975 *Thermal Vibrations in Crystallography* (Cambridge: Cambridge University Press)
[13] Hannon A C 1999 *Encyclopedia of Spectroscopy and Spectrometry* ed J Lindon, G Tranter and J Holmes (London: Academic) at press
[14] David W I F, Ibberson R M and Matthewman J C 1992 *Rutherford Appleton Laboratory Report* RAL-92-032
[15] Koester L and Yelon W B 1982 *Summary of Low Energy Neutron Scattering Lengths and Cross Sections* (Petten: Netherland Research Foundation, Department of Physics)
[16] Hauback B C, Fjellvåg H and Sakai N 1996 *J. Solid State Chem.* **124** 43–5
[17] Lisher E J and Forsyth J B 1971 *Acta Crystallogr.* A **27** 545–9